5A.3 COMPARISON OF THE DIURNAL CYCLE OF OUTGOING LONGWAVE RADIATION FROM A CLIMATE MODEL WITH RESULTS FROM ERBE

G. Louis Smith
National Institute of Aerospace, Hampton, VA

Anthony Slingo
Environmental Systems Science Centre, University of Reading, UK

Pamela E. Mlynczak
Science Applications International Corporation, Hampton, VA

David A. Rutan
Analytical Services and Materials Inc., Hampton, VA

1. INTRODUCTION

The diurnal cycle represents the response of the surface and atmosphere to solar heating on a time scale at which the details of surface properties, planetary boundary layer, clouds and precipitation are all important. In order to simulate well the diurnal cycle in all of the climatological regions of the Earth, a general circulation model must include each of these processes and their interactions. Whether the purpose is to model climate or to forecast the weather, these processes must be described well by the model, because of the nonlinearity of the system and the interactions of its components over a wide range of time and space scales. The accuracy with which a model replicates the diurnal cycle depends on how well the various processes are described by which solar radiation is absorbed at the surface and within the atmosphere, and the heat is subsequently transferred vertically by mixing processes and radiation and finally lost to space through the outgoing longwave radiation (OLR).

Several authors have examined the quality of the simulation of the diurnal cycle by climate models. Surface and related observations provide the most direct validation source, whether from dedicated field observations or existing meteorological networks (e.g. Betts and Jakob 2002, Dai and Trenberth 2004). Global satellite data also provide important observations, often in the form of narrow or broad-band thermal radiation fields that provide information on surface and cloud-top temperatures (e.g. Yang and Slingo 2001, Tian et al. 2004). Indirect information on the diurnal cycle of precipitation is frequently inferred from the radiation fields through regression relationships, but more direct comparisons have recently been made possible by the retrievals of rainfall rates produced from the Tropical Rainfall Measuring Mission, TRMM (Nesbitt and Zipser 2003, Collier and Bowman 2004). The OLR itself is sensitive not only to the temperature variations at the surface and its profile through the atmosphere but also to the humidity profile and clouds. Comparisons of the simulated diurnal cycle of the OLR with satellite measurements can thus provide a stringent test of many aspects of a model. Geostationary satellites are a particularly valuable resource because of the high time resolution available. For example, half-hourly data from Meteosat 7 were used by Slingo et al. (2004) to evaluate version HadAM3 of the Hadley Centre climate model.

While the details vary from model to model, a common theme in these comparisons is that the simulated convection and associated rainfall tend to peak far too early in the day, although the precise cause is still under investigation. A sensitivity to the frequency with which the radiative heating fields are updated in the model has also been found (e.g. Slingo et al. 2004). One difficulty in comparing the various studies is that different analysis techniques have often been employed to analyse the model output and observational data, including compositing by the local solar time (employed most frequently), Fourier analysis (e.g. Yang and Slingo 2001) and empirical orthogonal functions (Smith and Rutan 2003). While Fourier analysis efficiently extracts information on the diurnal and higher frequency harmonic components, there is a possibility that it could distort the time of maxima and minima for the strongly anharmonic diurnal variations typical over land. There is thus a need for a careful

Corresponding author address:
G. Louis Smith, Mail Stop 420, NASA Langley Research Center, Hampton, Virginia 23681
E-mail: g.l.smith@larc.nasa.gov
Phone: 757-864-5678, Fax: 757-864-7996

intercomparison of the various methods using the same input data, to quantify any such differences.

In this paper, we take the HadAM3 simulations analysed with the compositing technique by Slingo et al. (2004) and compare them with OLR data from the Earth Radiation Budget Satellite (ERBS) using the EOF analysis technique as employed by Smith and Rutan (2003). The purpose is both to extend the analysis of Slingo et al. (2004) to the global domain and to begin the process of methodological intercomparison mentioned above. ERBS was placed in an orbit with an inclination of 57^o, precessing through all local solar times every 72 days to provide the first direct observations of the diurnal cycle of the Earth's OLR and albedo (Harrison et al., 1983). The satellite provided five years of data from the scanning radiometer between 1985 and 1989. Harrison et al. (1988) used the scanner data to demonstrate the range of the diurnal cycle of the OLR. Smith and Rutan (2003) used these data to compute the diurnal cycles of OLR for 2.5^o latitude by 2.5^o longitude regions from 55^{o}S to 55^{o}N, which was the portion of the Earth observed by the ERBS. Those results provide information about the diurnal cycle of OLR beyond the view of Meteosat and extend the range of climatological regions for which comparisons can be made.

2. MODEL AND DATA

This study uses results from an integration of version HadAM3 of the Hadley Centre climate model, analysed by Slingo et al. (2004). The model has 30 vertical levels and a horizontal resolution of 2.5^o latitude by 3.75^o longitude. Full radiation calculations are made every model time step (half an hour), as opposed to the standard version of the model in which the full radiation computation is made every three hours. HadAM3 is the atmosphere-only version of the climate model, in which the model is forced with the observed sea surface temperatures and sea-ice extents. A full description of the model and of its simulations in this mode is given by Pope et al. (2000). Results are shown for July and for the northern summer season (June, July and August).

The ERBS measurements were limited to the latitude range from 55^{o}S to 55^{o}N. Further, in order to provide sufficient sampling of the diurnal cycle of each region within this domain, seasonal means were considered, i.e. for June, July and August. The HadAM3 model provides daily global coverage, so that diurnal cycles can be computed for the complete globe and for a single month. In addition to the ERBS results providing a validation for the model, the model can be used to provide global results, with the caveats noted in the comparison with the ERBS observations. Also, the model results are used to show how the seasonally-averaged diurnal cycles compare with those averaged over an individual month. Thus, the comparison of the diurnal cycle of OLR as computed by a GCM with the results from the precessing Earth Radiation Budget Satellite should reveal much about both the observational results and the model.

3. ANALYSIS PROCEDURE

Diurnal cycles were computed from ERBS measurements by Smith and Rutan (2003), henceforth denoted SR03, for 2.5^o regions from 55^{o}S to 55^{o}N, which requires 6336 regions for coverage. HadAM3 provides diurnal cycles for grid points covering 2.5^o latitude by 3.75^o longitude over the globe, which requires 6912 regions. The problem is how to compare several thousand diurnal cycle curves qualitatively and quantitatively. The approach used by SR03 was to use principal component (PC) analysis, which provides the most economical basis set possible, i.e. the first PC describes the maximum amount of variance of the diurnal cycle in time and space which is possible with one function, and each successive PC explains the maximum amount of variance of the residual. The set of PCs provide an orthogonal basis set for describing the time variation of the diurnal cycles. The diurnal cycle for each region is expressed by use of the PCs, for which the resulting coefficients are the empirical orthogonal functions EOFs, describing the geographical variation of the diurnal cycles.

The PC/EOF method produces a set of functions of local time (PCs), which are uncorrelated, i.e. statistically orthogonal, and a concomitant set of maps (EOFs) which are likewise uncorrelated. As such, these results are statistical descriptions, which are mainly useful to the extent that one can physically interpret them. This physical interpretation depends on the shape of the PC, the geographical location of the large EOF values and recognition of the processes which occur in these regions.

3.1 Computation of Model Diurnal Cycle

The version of HadAM3 analysed here computes the OLR at the "top of the atmosphere" every 30 minutes for every grid point, yielding 48 simulations each day. The diurnal cycle of a quantity for a region is calculated as the average departure at a given local time from the average daily-mean value for the region. Let $OLR(x,\tau,t)$ denote the OLR for region x for local time τ on day t, where τ has 48 values and t has up to 31 values. The monthly-average OLR for a given local time is then

$$\{OLR(x,\tau)\} = 31^{-1}\Sigma\ OLR(x,\tau,t)$$

and the daily-average OLR for the region during the month is

$$\{\{OLR(x)\}\} = 48^{-1}\ \Sigma\ \{OLR(x,\tau)\}$$

The diurnal cycle for region x is then

$$D(x,\tau) = \{OLR(x,\tau)\} - \{\{OLR(x)\}\}$$

A consequence of this definition is that the average of the diurnal cycle over a day is zero.

3.2 Principal Component Analysis

The first step of the PC analysis is to compute the covariance matrix as

$$\Gamma(\tau,\tau') = \Sigma\ w(x)\ D(x,\tau)\ D(x,\tau')$$

where $w(x)$ is the area weighting for the x-th region and the summation is over all regions. Because τ takes on values from 1 to 48, the covariance matrix is 48x48. The eigenvectors of the covariance matrix are the principal components $PC_n(\tau)$, where $n \in [1,48]$. The corresponding empirical orthogonal functions provide the geographic distribution and are computed as

$$EOF_n(x) = \Sigma\ D(x,\tau)\ PC_n(\tau)$$

where the summation is over τ. The diurnal cycle for a region can be expressed as

$$D(x,\tau) = \Sigma\ PC_n(\tau)\ EOF_n(x)$$

where the summation is over n. The results of these computations with the HadAM3 model and comparisons with ERBS observations are discussed in the following section.

4. RESULTS FOR LAND

The diurnal cycle of OLR over land is much greater than over ocean, due to the much larger effective heat capacity of the oceans. SR03 therefore partitioned their analysis into land and ocean, so that the variation of OLR over land would not overwhelm that over ocean. Also, the physics of the diurnal cycles over ocean differ from those over land, so the partitioning of the globe into land and ocean permits the analysis method to show these differences more easily. That approach is also used here. In the partitioning, regions containing both land and ocean are excluded from the analysis.

The PCs and EOFs of the HadAM3 OLR data set were first computed for July, then for summer and over the ERBS domain (i.e. averaged over June, July and August between 55°S to 55°N), in order to compare directly with the ERBS results.

4.1 Variances over land

The root-mean-square variance (RMS) is computed as the square root of the trace of $\Gamma(\tau,\tau')$, which is the sum of the squares of all $D(x,\tau)$ values for all x and τ. Table 1 lists the RMS for the model diurnal cycle for the globe for July, for the model over the ERBS domain of 55°S to 55°N for summer (June, July and August) and for the ERBS results for summer. For the globe, the RMS of the modelled diurnal cycle is 14.5 Wm^{-2} in July. For the ERBS domain in summer, the model's RMS is slightly higher at 16.2 Wm^{-2}, because the regions with latitudes higher than 55° have small diurnal cycles compared with lower latitudes. The ERBS result is 13.3 Wm^{-2}, so the model has a larger diurnal cycle over land than the satellite data.

Order	Model Global July	Model ERBS Domain, Summer	ERBS Summer
1	0.856	0.887	0.757
2	0.075	0.057	0.101
3	0.037	0.033	0.021
4	0.011	0.009	0.017
5	0.005	0.004	0.011
Sum of 5 terms	0.984	0.990	0.907
RMS	14.6	16.2	13.3

Table 1. Root-mean-square of outgoing longwave radiation (W m^{-2}) and eigenvalues for land.

The eigenvalues of the covariance matrix normalized by the trace are also listed in Table 1 for the three cases. The normalized eigenvalues represent the fraction of variance which is described by each PC and thus quantify the importance of each term. The model eigenvalues decrease more rapidly than the measured, so that fewer terms are required to describe the model diurnal cycles than for the observed, indicating that the diurnal cycles which are observed by satellite have a greater variety than those computed by the model. For the model, 99% of the variance over the ERBS domain can be described by five terms, whereas for the observed diurnal cycles, five terms describe only 91% of the variance.

4.2 Principal Components from model for land in global domain for July

Figure 1 shows the first three principal components from the model, for the entire globe for July. The first principal component shows the OLR decreasing slowly from sunset to sunrise, with a sinusoidal increase beginning at sunrise, approximating the cosine of the solar zenith angle. Table 1 shows that PC-1 describes 86% of the model variance of OLR over land. Figure 2 shows the first empirical orthogonal function EOF-1, which is the geographically dependent coefficient for PC-1. Over the deserts of North Africa, the Middle East and southern Asia, EOF-1 exceeds 2. The shape of the PC-1 curve in fig. 1 and the distribution of the coefficient in fig. 2 show that this PC picks up the classic signature of the strong response of surface temperatures to the solar heating over cloud-free land. For such regions, particularly the deserts, the OLR closely follows the surface temperature, with a maximum just after noon and a slow cooling through the night to a minimum just before dawn. This interpretation is supported by the fact that plots of the OLR obtained directly from the model over the Sahara (not shown here) are identical in shape to that for PC-1 shown in fig. 1. On the other hand, it is noteworthy that there are substantial regions on fig. 2 where the coefficient is negative, particularly over the monsoon areas such as equatorial South America, West Africa, India and Southeast Asia. This result will be discussed with regard to fig. 9.

The PC-2 is a sine wave, accounting for 7.5% of the variance of the OLR diurnal cycle, and fig. 3 shows EOF-2. Combined with a negative EOF value, PC-2 will shift the peak OLR to an earlier time of day, as happens over areas with afternoon cloudiness. This is the case where the deep convection of central Africa has moved north of the Equator in July. In such regions, PC-1 may be interpreted very simply as the direct response of the OLR to the surface heating under clear skies, while PC-2 represents the modification introduced by the diurnal cycle of the resulting cloudiness. In contrast, many regions in fig. 3 show positive EOF values, which shift the peak heating to later in the day. This is particularly widespread away from the equator, suggesting that the effective heat capacity of the surface in these regions is larger than that over the deserts, delaying the maximum surface temperature and hence the maximum OLR.

PC-3 has peaks at the null points of PC-1, so a combination of the two will broaden or narrow the peak of the diurnal cycle. This behavior is expected as a response to the dependence of the length of the day on the latitude. In addition, the shape of PC-3 is very similar to that shown in fig. 15(d) of Slingo et al. (2004) over South America; in this case the behavior is caused by a combination of surface heating and the oscillatory nature of the resulting convective cloudiness. PC-3 thus picks up some of the more subtle signals not represented by a combination of PC-1 and PC-2.

These first three PCs and their EOFs account for 97% of the variance of the modelled OLR diurnal cycle over the globe.

4.3 Comparison of model and ERBS for boreal summer

In order to compare the model diurnal cycle with results from the satellite measurements, the domain was limited to within 55^o of the equator and the average diurnal cycle for June, July and August was computed. Table 1 shows that the model PC-1 describes 89% of the variance, or slightly more for the ERBS domain than for the global case, compared to 76% for the ERBS PC-1. Figure 4 compares PC-1 from the model and from ERBS. The two results are very similar; for example, the model curve has an amplitude of 27 Wm^{-2} compared with 30 Wm^{-2} for ERBS. However, there are some important differences. The satellite result is very nearly symmetric about noon, with no discernible decrease of the OLR during the night. This result was also found by Minnis and Harrison (1984), using data from the GOES window channel. In contrast, the model result is skewed such that the maximum occurs at about 1330 hours, which is more intuitive than the symmetry of the satellite result, since it represents the delay caused by the finite heat capacity of the surface. In addition, the model PC-1 has large curvature near sunrise and sunset, whereas the ERBS PC-1 is more rounded, indicating an increase prior to 0600 hours. This early increase of ERBS PC-1 can be explained as the result of the variation of sunrise and sunset times with latitude, which is explained by PC-3. The model result has a higher variance for PC-3.

EOF-1 from the ERBS measurements is shown in fig. 5. The map of EOF-1 for the model over the ERBS domain for boreal summer differs little from that shown in fig. 2 for the model globe during July and is therefore not shown here. Compared to the ERBS EOF-1, the model result has similar patterns over deserts and surrounding regions. The very high model values over the deserts do not appear in fig. 5, but the major difference between the two maps is the appearance of negative values over large areas in the model EOF-1, noted in discussion of fig. 2 and to be explained further in conjunction with fig. 9.

Figure 6 shows the model PC-2 and the ERBS PC-2. The two curves agree quite well, especially considering the differences noted earlier for PC-1, which can cause differences to be transferred to higher order PCs, and the fact that the model PC-2 accounts for only 5.7% of the variance, compared to 10% for the ERBS PC-2. However, in each case the primary effect is to describe the lead or lag of a given region compared to the gross average, so the similarity of shape is perhaps not surprising. Likewise, the model and satellite PC-3, shown in fig. 7, are similar, if one regards PC-3 as a Fourier wavenumber 2 and ignores the higher frequency variations.

The diurnal cycles as computed for two sites by the HadAM3 model and from ERBS data are now considered. Figure 8a shows the diurnal cycle for a region in the Sahara Desert (22^{o}N, 22^{o}E) from ERBS data and fig. 8b shows the diurnal cycle as computed by the model. The diurnal cycle for this region is the strongest on Earth. Figures 8a and 8b show a maximum of 340 W-m^{-2} for ERBS and 350 W-m^{-2} for the model, and a minimum of about 285 W-m^{-2} for both. The maximum for both cases occurs near 13:00 LST. Also shown for each case is the diurnal cycle reconstructed from the principal components and EOFs using one and two terms, i.e., PC-1 x EOF-1 and PC-1 x EOF-1 + PC-2 x EOF-2. For the ERBS case the first term reproduces most of the features of the diurnal cycle, except that PC-1 for ERBS is symmetric about noon. Addition of the second term shifts the peak to the proper time and gives a close fit, showing that higher order terms are quite small. For the model case, the first term gives an excellent representation of the diurnal cycle and even the second term is very small. A region in the intertropical convergence zone ITCZ (5^{o}N, 30^{o}E) is next examined in fig. 9a and 9b. The diurnal cycles for the Sahara Desert site were very smooth, but this ITCZ location has a very irregular diurnal cycle for the ERBS case and a complex shape for the model case. These irregularities are due to the limited sampling for both the ERBS and the model of the chaotic clouds over the region. Because of the irregular shape, two terms provide only a rough fit to the diurnal cycles. Interestingly, the model case has a negative EOF-1 value, because of the mid-day minimum of OLR due to convection between 10:00 and 16:00 LST. This minimum in the model OLR is several hours before the convection causes the OLR minimum in the ERBS data and is a symptom of model errors discussed by Slingo et al. (2004).

The decomposition of a set of functions, such as the diurnal cycles of OLR for the set of regions, onto a basis set provides a mathematical description of the functions. The use of principal components, e.g. rather than Fourier analysis, permits the data to define the basis set in such a manner that each PC describes as much of the remaining variance as possible. For the ERBS data, PC-1 (with 76% of the variance) is symmetric about noon, and PC-2 (with 10% of the variance) describes the shift of peak heating to the afternoon for regions which are clear in the afternoon and to morning for regions which are clear in the morning and develop afternoon cloudiness. For the model data, the single function which describes the maximum possible variance (87%) has an afternoon peak near 1330 hours. If the convection in the model occurred later in the day, it would increase the variance in PC-2 and shift the peak of PC-1 toward noon.

5. RESULTS FOR OCEAN

The surface temperature of land undergoes large changes during the day, especially over deserts, resulting in large changes in OLR over the course of a day. Due to the immense heat capacity of the ocean, the temperature change of its surface is quite small during the day, and the OLR change due to temperature change is likewise small. Most of the diurnal variation of OLR over ocean is due to cloud formation and dissipation.

5.1 Variances over ocean

Table 2 shows that the RMS for the diurnal cycle over ocean for the model is 4.2 Wm^{-2} for the globe, compared to 4.0 Wm^{-2} for the ERBS domain, implying slightly more variability in latitudes above 55^o than in lower latitudes. This is the reverse of the situation over land. The ERBS result shows an RMS of 5.9 Wm^{-2}, indicating that the diurnal cycle of OLR is greater than that computed by the model. The sum of the first five terms is much smaller for ocean than for land, so the variance as a function of the order of the term converges far more slowly for ocean than for land for both the model and ERBS. The larger number of terms required to describe the diurnal cycle over ocean shows that the variety of diurnal cycles is greater than over land. For ERBS, the sum of the first five terms is only 0.47, thus the complexity is greater for ERBS than for the model, as was found over land.

Order	Model Global July	Model ERBS Domain, Summer	ERBS Summer
1	0.553	0.655	0.155
2	0.246	0.227	0.107
3	0.030	0.028	0.091
4	0.026	0.024	0.067
5	0.013	0.006	0.054
Sum of 5 terms	0.868	0.940	0.474
RMS	4.2	4.0	5.9

Table 2. Root-mean-square of outgoing longwave radiation (W m^{-2}) and eigenvalues for ocean.

5.2 Comparison of model and ERBS over ocean in July

PC-1 and EOF-1 will be compared for the ocean case. However, the first term for the model accounts for 55% of the variance over the globe and 66% of the variance over the ERBS domain, whereas for ERBS the first term accounts for only 16% of the variance; even the first five terms together account for only 47%. Thus, the PCs and EOFs cannot be expected to agree very well.

Figure 10 shows PC-1 for the diurnal cycle of OLR over the oceans for the model and for the ERBS results. For the model, PC-1 is very nearly sinusoidal, with a peak near 1600 hours and minimum near 0400 hours. The PC-1 from ERBS increases during the morning with a peak at noon and decreases to a minimum at 2000 hours. There is a subsidiary maximum just after nidnight, followed by a decrease to 0600. The increase during the night may be due to clearing of clouds which have formed during the day.

Figure 11 shows the map of EOF-1 for the model results for ocean. The diurnal cycle is strong at low latitudes, coincident with the convectively active regions, and decreases with increasing latitude. There are maxima near some of the coasts, which may be due to a residual influence of the diurnal cycle over the adjacent land regions. EOF-1 for ERBS, in fig. 12, shows negative values over the western oceans and strong positive values for the eastern oceans in the Northern Hemisphere (summer) but not in the Southern Hemisphere (winter). These features do not appear in the model results. The model shows a significant diurnal cycle in the regions of the intertropical convergence zones, which does not appear in the ERBS results. Both the model and ERBS show a strong positive EOF-1 value over the Indian Ocean at the Equator.

For the model, PC-2 describes 25% of the variance over the globe and 23% over the ERBS domain and for ERBS PC-2 accounts for 11% of the variance. Figure 13 shows PC-2 for the model and for ERBS. The model PC-2 is a sinusoid 90^o out of phase with PC-1, the effect of which is to give a sine wave at each region, with the phase varied by PC-2. The model results can be duplicated with a linear model using a single mass at each grid point, with the mass adjusted to match the phase shift described by PC-2. The ERBS PC-2 is a wave 2. This is a non-linear response of the system to the cycle of solar forcing. Again, in order to explain the ERBS results, one needs to examine cloud data.

6. CONCLUSIONS

The method of Principal Component Analysis has been used to extract the features of the diurnal cycle of outgoing longwave radiation (OLR) as generated by the version HadAM3 of the Hadley Centre model and to compare these features with those derived from the measurements from the Earth Radiation Budget Experiment aboard the Earth Radiation Budget Satellite (ERBS). The diurnal cycle of OLR differs in range and physical mechanisms over land and over ocean, so the Earth is partitioned into land and ocean for the analysis.

Over land, the root-mean-square (RMS) of the cycles are comparable, with 16.2 Wm^{-2} for the model and 13.3 Wm^{-2} for ERBS. The first principal component (PC) for the model agrees well with that from ERBS and accounts for 89% of the variance of OLR for the model and 76% for ERBS. However, the model PC-1 has a peak near 1330 hours rather than the symmetry about noon of the ERBS PC-1 and decreases at night, whereas the ERBS result does not. Intuitively both of these features seen in the model result are expected, so more research is needed to resolve this difference. The empirical orthogonal component map corresponding to PC-1 for the model agrees reasonably well with the map for ERBS.

For the ocean, the diurnal cycle is much smaller than over land, and the RMS is 4.0 Wm^{-2} for the model and 5.9 Wm^{-2} for ERBS. Also, the variety of patterns to be described by the PCs is considerably greater over the ocean for both the model and ERBS than over land. For ocean the model PC-1 is a simple sine wave, whereas the ERBS PC-1 has a more irregular structure.

Reasons for differences between the model and satellite-derived results which have been observed in this study are discussed. The model computes convection too early in the day, which reduces the variance of the second principal component and causes the first principal component to peak later in the day. Over the region covered by the Meteosat-8 satellite, the Geostationary Earth Radiation Budget (GERB) instrument (Harries et al., 2005) now provides data with excellent temporal sampling with which to study these issues.

7. ACKNOWLEDGEMENTS

GLS, PEM and DAR were supported in this work by the Earth Sciences Enterprise of NASA by contract with the Langley Research Center (LaRC) of NASA. ERBE data for computation of the diurnal cycle of outgoing longwave radiation were supplied by the Atmospheric Sciences Data Center of LaRC.

8. REFERENCES

Betts, A. K. and C. Jakob, 2002: Evaluation of the diurnal cycle of precipitation, surface thermodynamics, and surface fluxes in the ECMWF model using LBA data. *J. Geophys. Res*., *107*, 8045, doi:10.1029/2001JD000427.

Collier, J. G. and K. P. Bowman, 2004: Diurnal cycle of tropical precipitation in a general circulation model. *J. Geophys. Res., 109,* D17105, doi:10.1029/2004JD004818.

Dai, A. and K. E. Trenberth, 2004: The diurnal cycle and its depiction in the Community Climate System model. *J. Clim., 17*, 930-951.

Harries, J.E. and 42 others, 2005. The Geostationary Earth Radiation Budget (GERB) project. *Bull. Amer. Meteorol. Soc*., *86*, 945-960.

Harrison, E. F., D. R. Brooks, P. Minnis, B. A. Wielicki, W. F. Staylor, G. G. Gibson, D. F. Young and F. M. Denn, 1988: First estimates of the diurnal variation of longwave radiation from the multiple-satellite Earth Radiation Budget Experiment (ERBE). *Bull. Amer. Met. Soc., 69*, 1144-1151.

Harrison, E. F., P. Minnis, and G. G. Gibson, 1983: Orbital and cloud cover sampling analyses for multi-satellite Earth radiation budget experiments, *J. Spacecraft and Rockets, 20*, 491-495.

Minnis, P. and Harrison, E F., 1984: Diurnal Variability of Regional Cloud and Clear-Sky Radiative Parameters Derived from GOES Data, Part I: Analysis Method*. J. Climate Appl. Meteorol., 23*, 993-1011.

Nesbitt, S.W. and Zipser, E.J., 2003. The diurnal cycle of rainfall and convective intensity according to three years of TRMM measurements. *J. Clim*., *16***,** 1456-1475.

Pope, V. D., M. L. Gallani, P. R. Rowntree and R. A. Stratton, 2000: The impact of new physical parametrizations in the Hadley Centre Climate Model: HadAM3. *Climate Dyn.*, *16,* 123–146.

Slingo, A., K. I. Hodges and G. J. Robinson, 2004: Simulation of the diurnal cycle in a climate model and its evaluation using data from Meteosat 7. *Q. J. R. Meteorol. Soc., 130,* 1449-1467.

Smith, G. L. and D. A. Rutan, 2003: The diurnal cycle of outgoing longwave radiation from Earth Radiation Budget Experiment measurements. *J. Atmos. Sci., 60*, 1529-1542.

Tian, B., B. J. Soden and X. Wu, 2004: Diurnal cycle of convection, clouds and water vapor in the tropical upper troposphere: satellites versus a general circulation model. *J. Geophys. Res., 109,* D10101, doi:10.1029/2003JD004117.

Yang, G.-Y. and J. Slingo, 2001: The diurnal cycle in the tropics. *Mon. Weather Rev.*, *129,* 784-801.

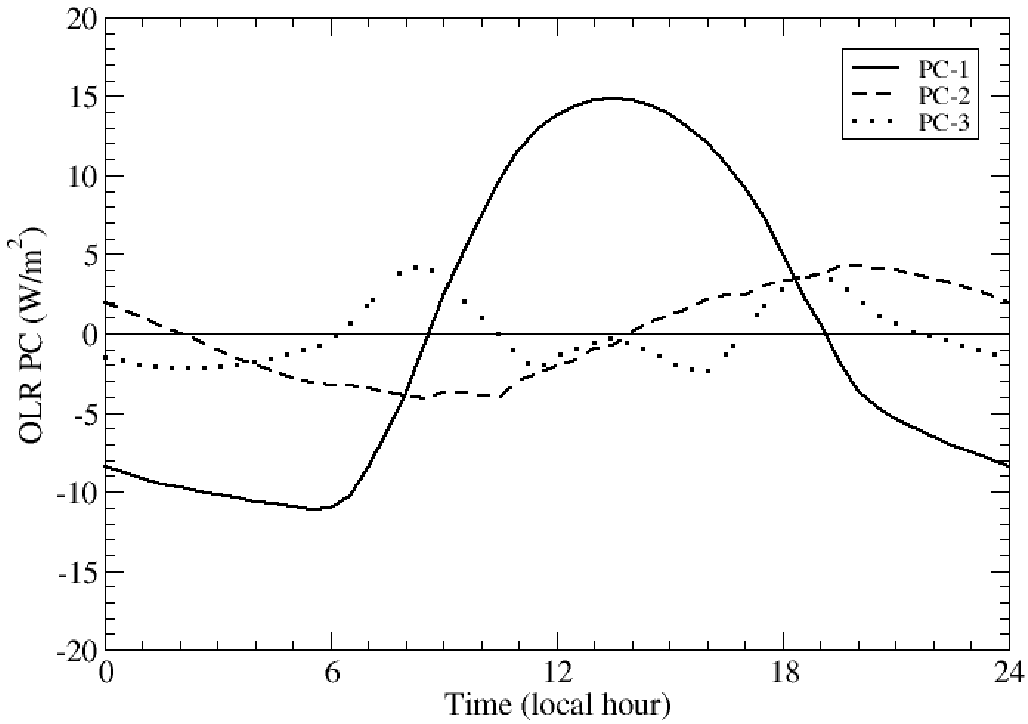

Figure 1. First three principal components of diurnal cycle of OLR of model for global domain of land during July.

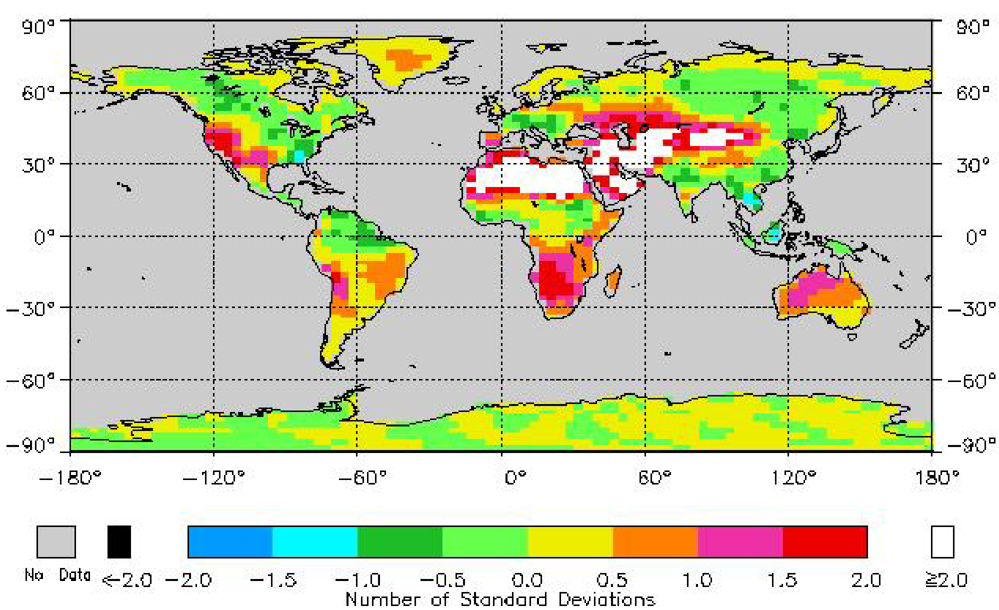

Figure 2. Map of first empirical orthogonal function of diurnal cycle of OLR of model for global domain of land during July.

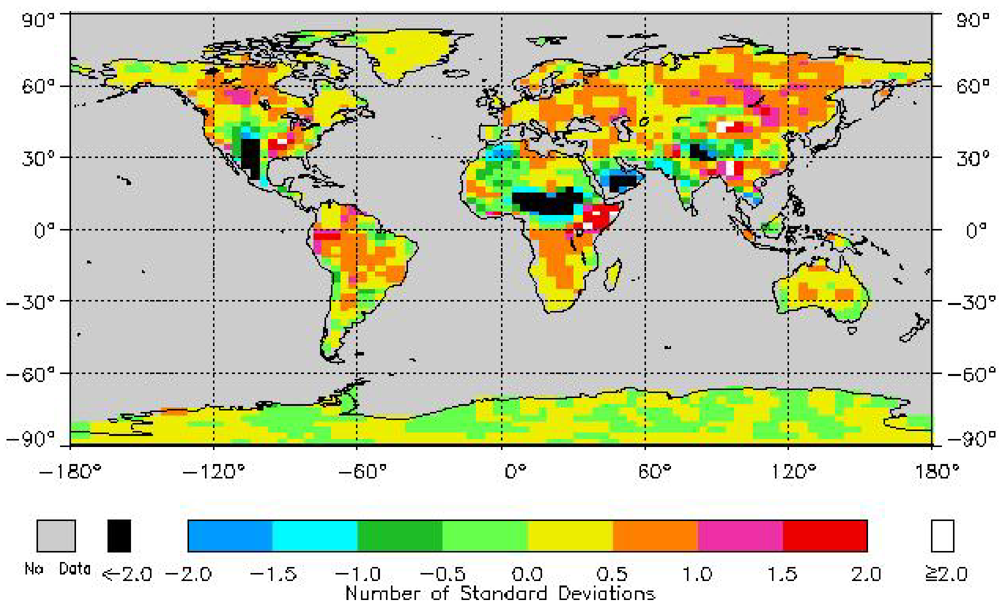

Figure 3. Map of second empirical orthogonal function of diurnal cycle of OLR of model for global domain of land during July.

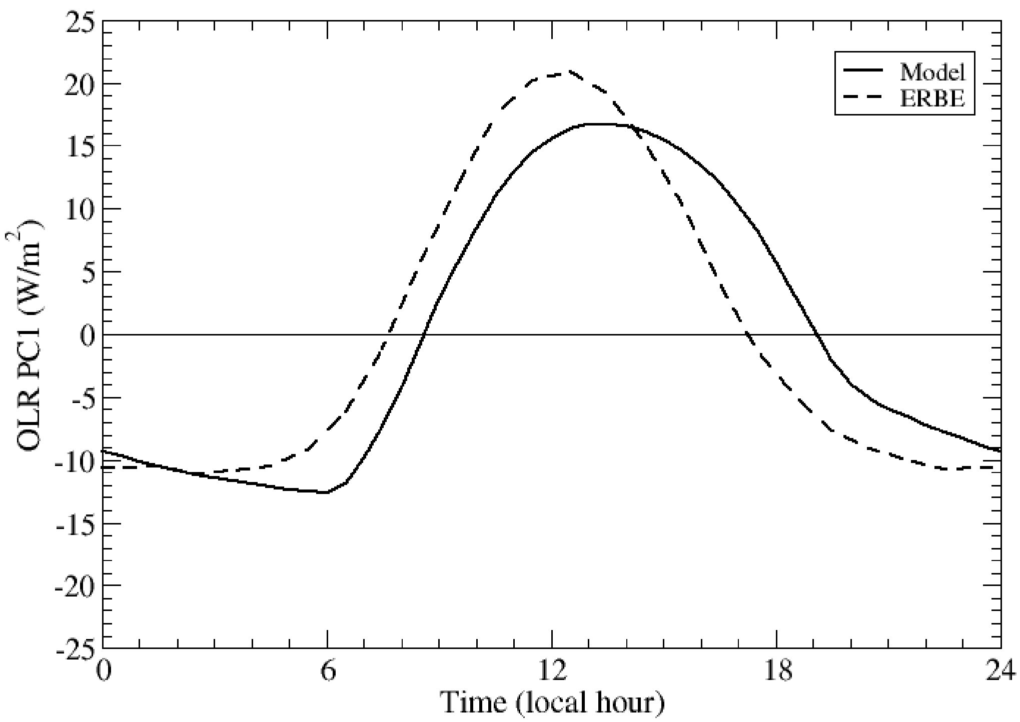

Figure 4. First principal component of diurnal cycle of OLR for ERBS result and of model for 55^{o}S to 55^{o}N for land during June, July and August.

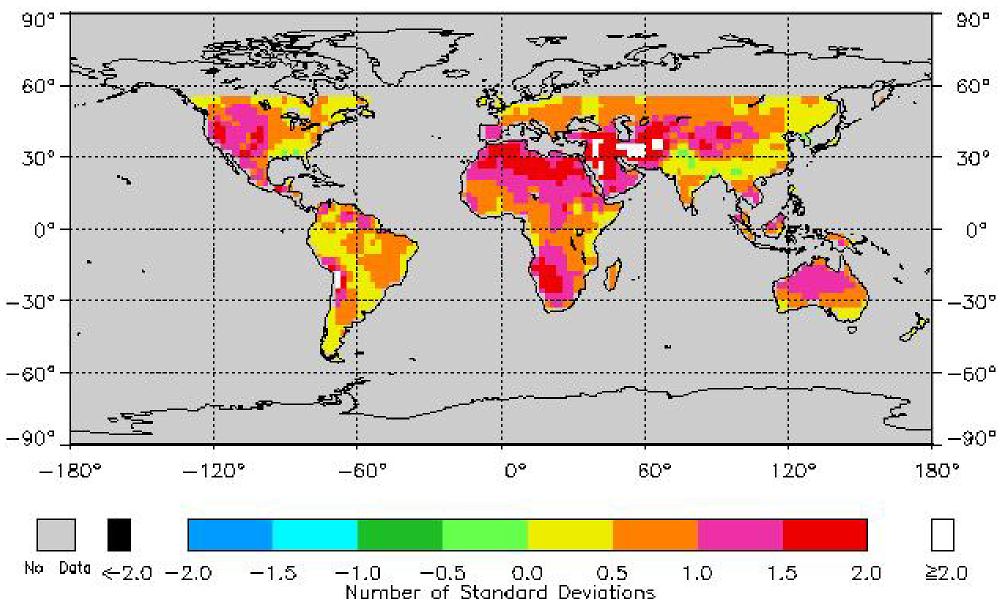

Figure 5. Map of first empirical orthogonal function of diurnal cycle of OLR as computed from ERBS measurements of land during June, July and August.

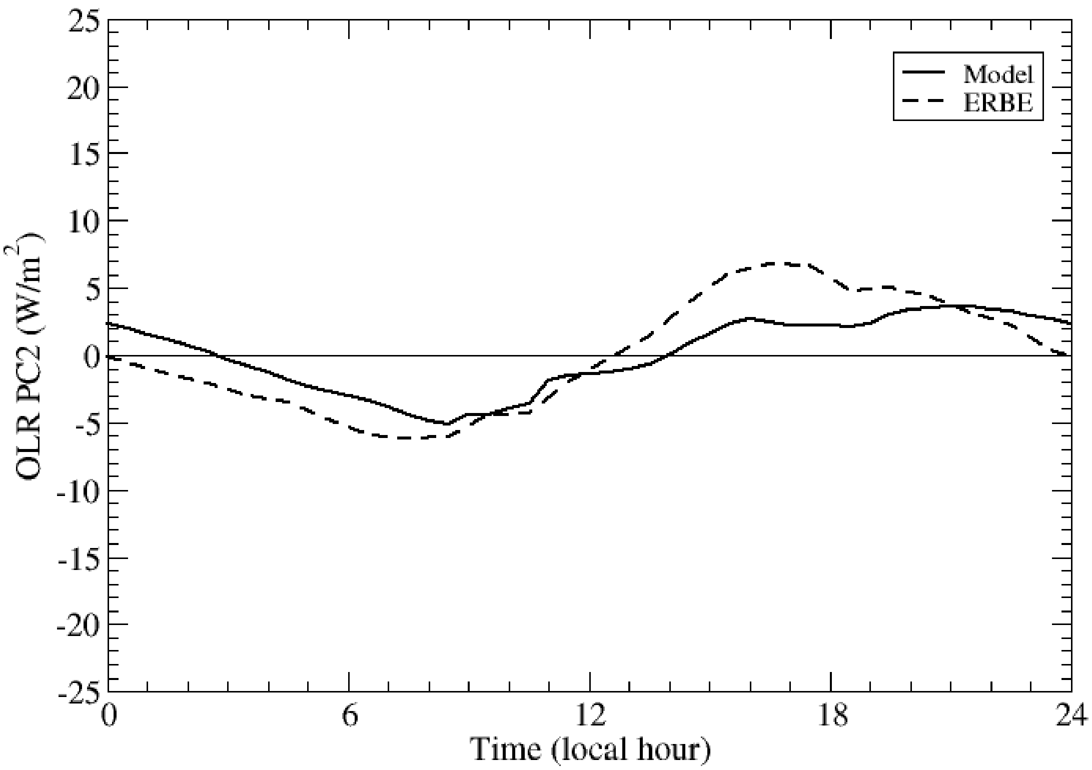

Figure 6. Second principal component of diurnal cycle of OLR of ERBS result and of model for 55^{o}S to 55^{o}N for land during June, July and August.

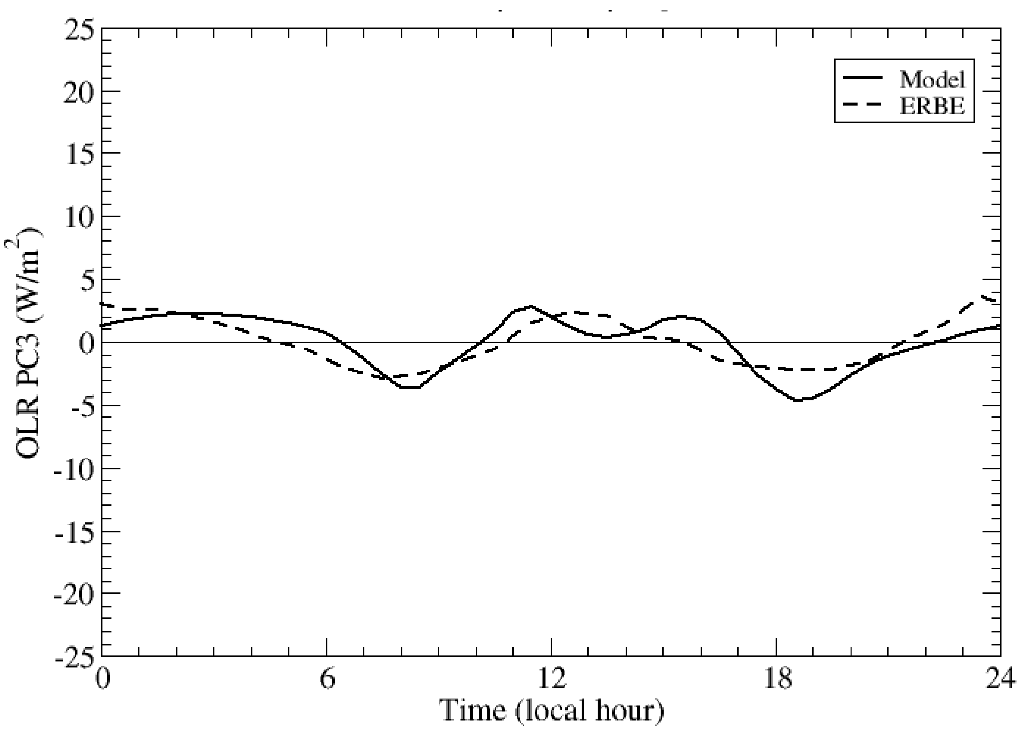

Figure 7. Third principal component of diurnal cycle of OLR of ERBS result and of model for 55°S to 55°N for land during June, July and August.

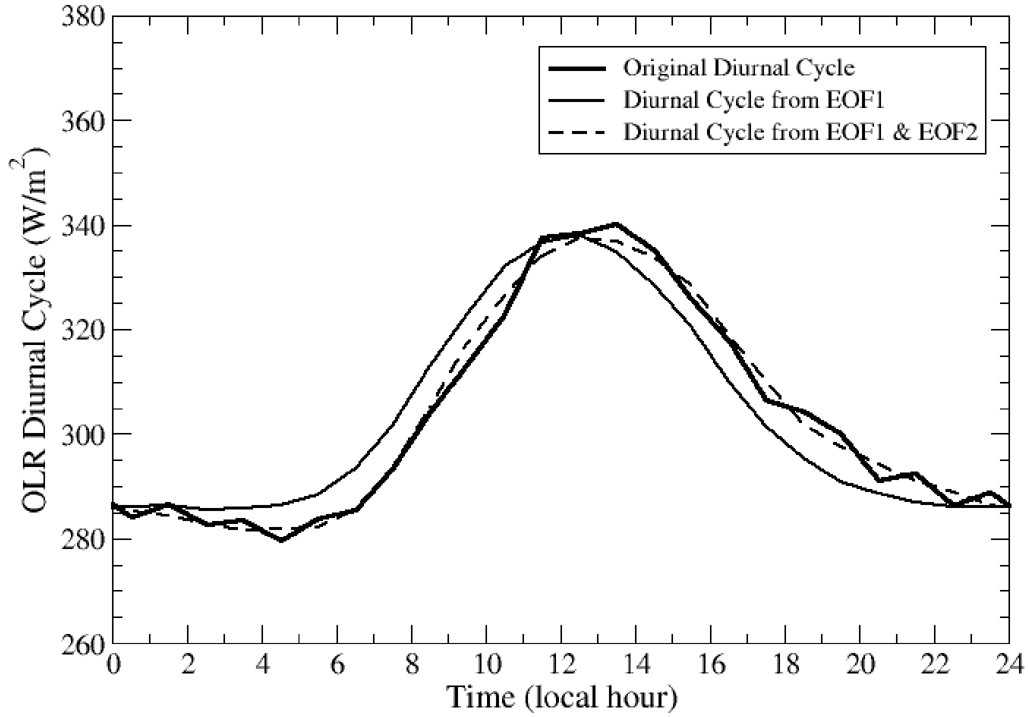

Figure 8a. Diurnal cycle of OLR over the Sahara Desert (22^{o}N, 22^{o}E) and representation using one and two terms of principal components and EOFs from ERBS.

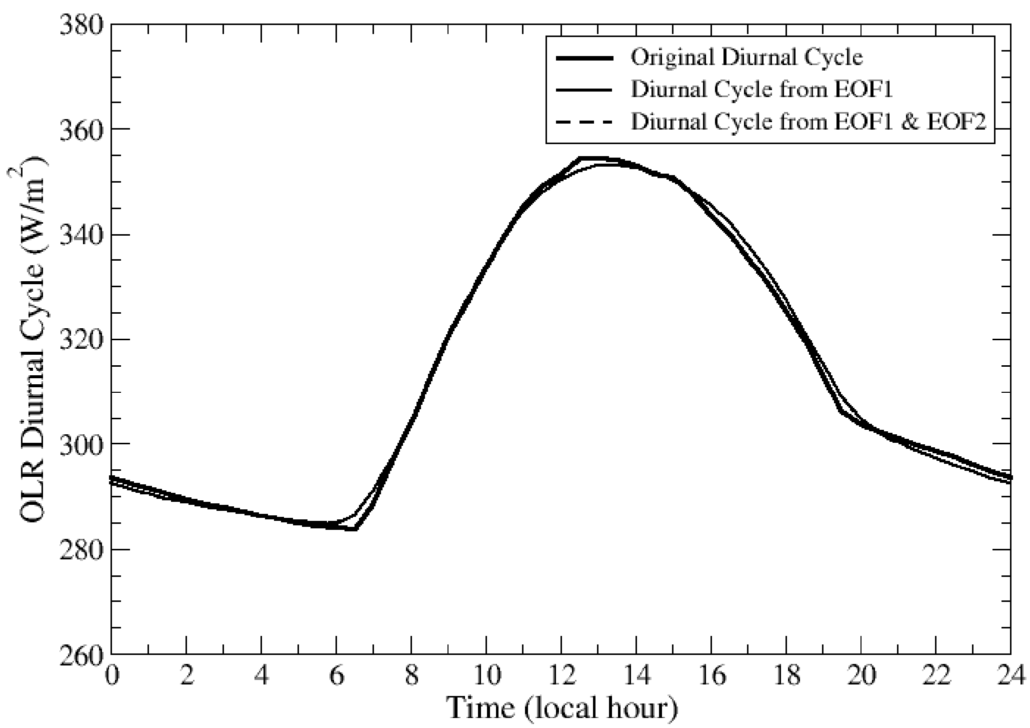

Figure 8b. Diurnal cycle of OLR over the Sahara Desert (22^{o}N, 22^{o}E) and representation using one and two terms of principal components and EOFs from Hadley model.

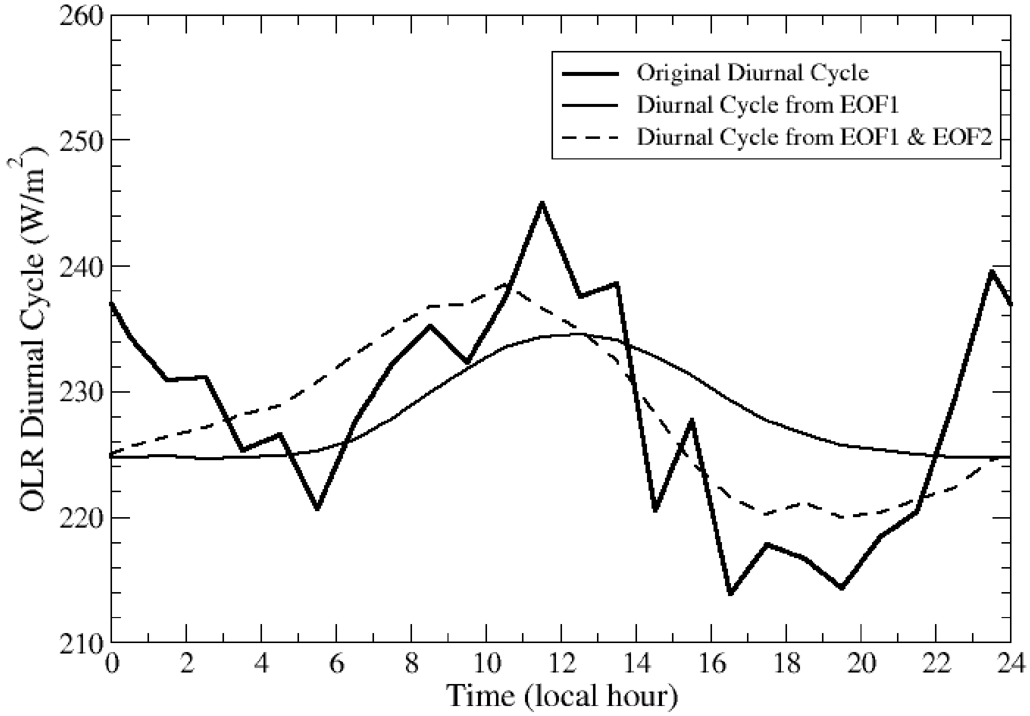

Figure 9a: Diurnal cycle of OLR over the intertropical convergence zone in Central Africa (5^{o}N, 30^{o}E) and representation using one and two terms of principal components and EOFs from ERBS.

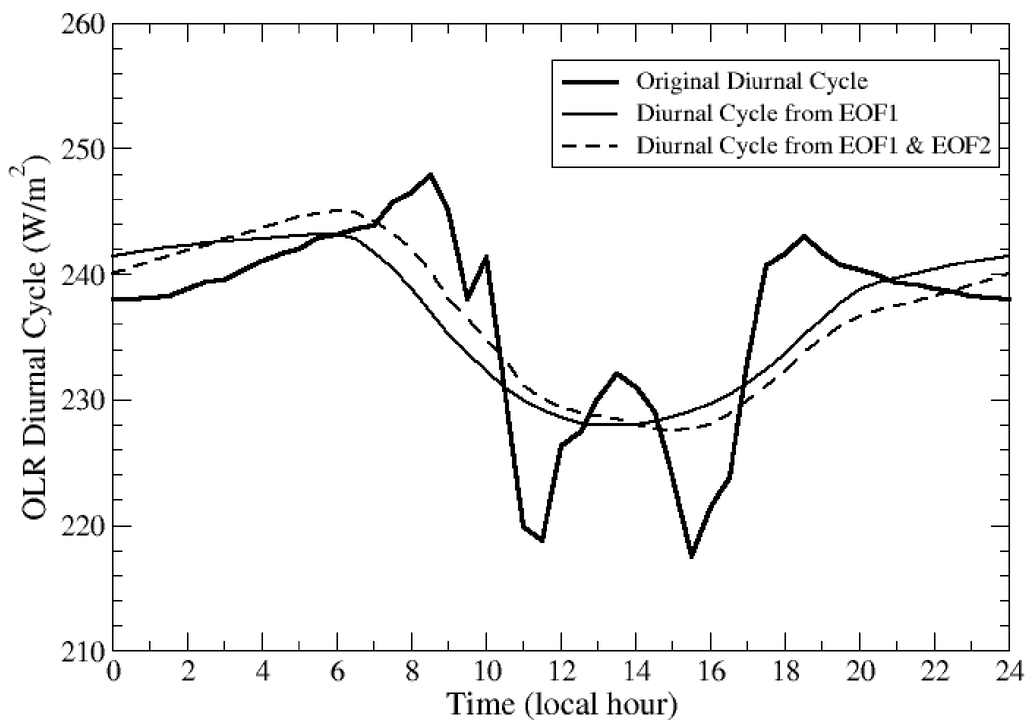

Figure 9b: Diurnal cycle of OLR over the intertropical convergence zone in Central Africa (5^{o}N, 30^{o}E) and representation using one and two terms of principal components and EOFs from Hadley model.

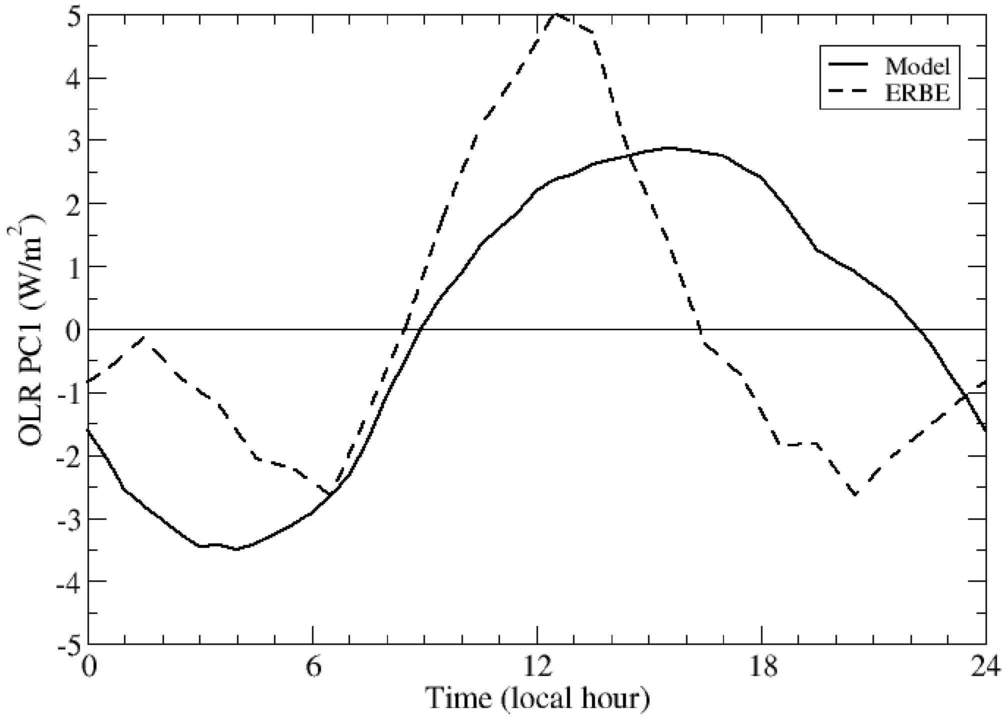

Figure 10. First principal component of diurnal cycle of OLR for ERBS result and of model for 55^{o}S to 55^{o}N for ocean during June, July and August.

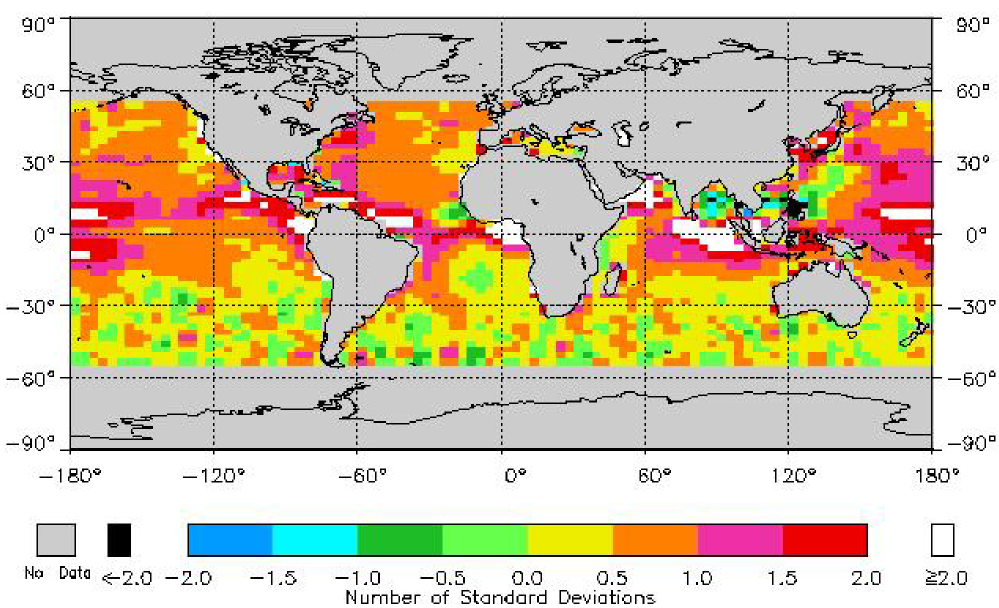

Figure 11. Map of first empirical orthogonal function of diurnal cycle of OLR for model results for ocean during June, July, and August.

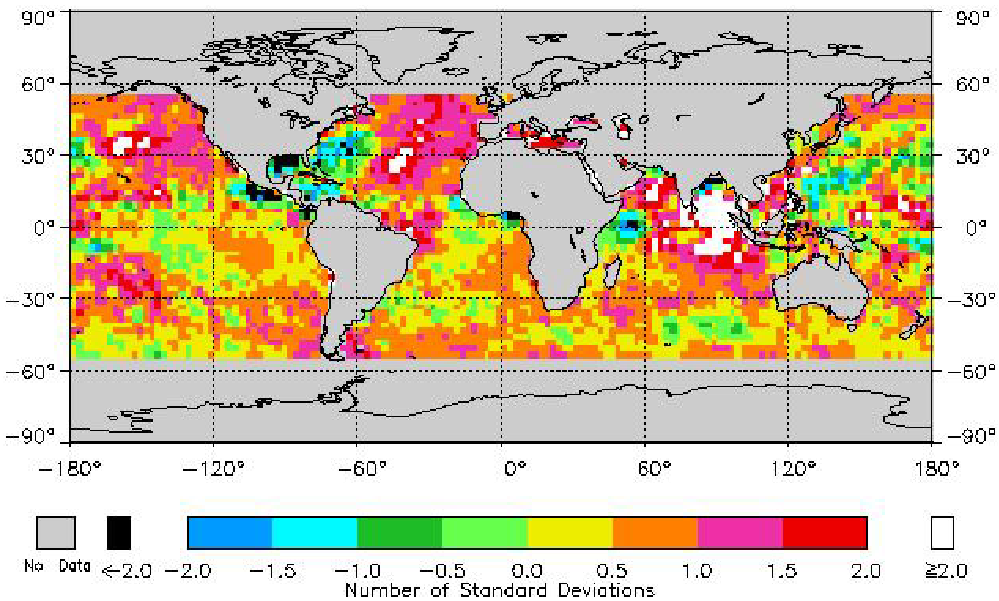

Figure 12. Map of first empirical orthogonal function of diurnal cycle of OLR as computed from ERBS measurements of ocean during June, July and August.

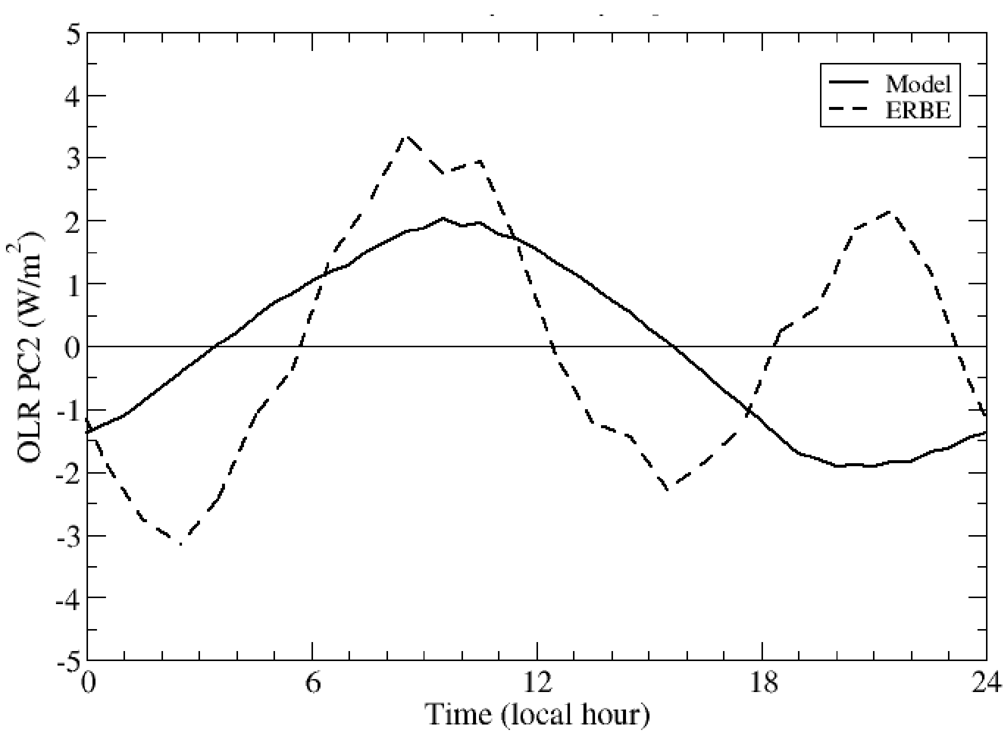

Figure 13. Second principal component of diurnal cycle of OLR of ERBS result and of model for 55^{o}S to 55^{o}N for ocean during June, July and August.